

Multi-Scale Architectures Matter: On the Adversarial Robustness of Flow-based Lossless Compression

Yi-chong Xia, Bin Chen, Yan Feng, Tian-shuo Ge

Keywords: Flow models, Lossless Compression, Adversarial Attack, Lipschitz Property

Abstract

Flow-based models are attractive in lossless image compression due to their exact likelihood estimation on entropy coding. In practice, the lossless compression ratio affects the storage cost of data with high fidelity. However, the robustness and efficiency trade-off of flow-based deep lossless compression models has not been fully explored. In this paper, we characterize the trade-off of flow-based deep lossless compression theoretically and empirically. Specifically, we show that flow-based models are susceptible to adversarial examples in terms of dramatic change in compression ratio. In theory, we demonstrate that the fragile robustness of the flow-based model is caused by its intrinsic multi-scale architectures that lack the desirable Lipschitz property. Based on the theoretical insight, we develop a stronger attack, i.e., Auto-Weighted Projected Gradient Descent (AW-PGD), on flow-based lossless compression algorithms, which is more effective and can generate more universal adversarial examples. Furthermore, we propose a novel flow-based lossless compression model, Robust Integer Discrete Flow (RIDF), which can achieve comparable robustness as adversarial training without loss of compression efficiency. Our experiments show that the PGD algorithm will fall into local extreme values when attacking the compression model. Our attack method can effectively escape the saddle point and attack the compression task more effectively. Moreover, our defense method can greatly improve the invulnerability of the flow-based compression model with almost no sacrificing of clean model performance.

Introduction

As a probabilistic modeling technique, the flow-based model has demonstrated remarkable potential in the field of lossless compression (Hoogeboom et al. 2019; Berg et al. 2020; Ho, Lohn, and Abbeel 2019; Zhang et al. 2021b,a). Compared with other deep generative models (eg. Autoregressive, VAEs) (Kingma, Abbeel, and Ho 2019; Townsend et al. 2019; Salimans et al. 2017; Chen et al. 2018) that explicitly model the data distribution probabilities, flow-based models perform better due to their excellent probability density estimation and satisfactory inference speed. In flow-based models, multi-scale architecture provides a shortcut from the shallow layer to the output layer, which significantly reduces the computational complexity and avoid performance degradation when adding more layers. This is essential for con-

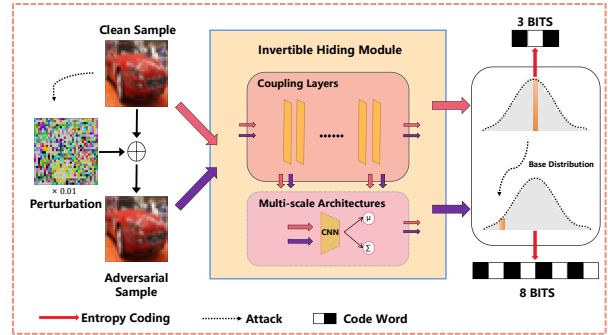


Figure 1: An example of an adversarial attack on a flow-based compression model. Although this adversarial noise is almost invisible, it successfully causes a dramatic shift in the likelihood of the flow model output and reduces the compression ratio from 2.5 to 1 (uncompressed).

structing an advanced flow-based learnable bijective mapping. Furthermore, the lightweight requirement of the model design in practical compression tasks suggests that flows with multi-scale architecture achieve the best trade-off between coding complexity and compression efficiency.

Despite recent works (Zhang et al. 2021b; Hoogeboom et al. 2019; Berg et al. 2020) mainly focus on designing more expressive architectures within the flow-based lossless compression models, the robustness of the inner architectures is ignored. This poses a potential security threat in cloud and streaming platforms with lossless compression codecs consisting of unreliable architectures. For example, the cloud and streaming platforms can be vulnerable to flow attack when the volume of transmitted or stored data grows rapidly controlled by the adversary as shown in Fig. 1. The clean sample is assigned with a short code length 3 bits estimated with high probability from a known probability distribution by the flow-based compression model. But the adversary can add a slight perturbation to induce the perturbed image being wrongly estimated with low probability, i.e. with longer code length 5 bits. This makes it problematic to deploy flow-based lossless compression codes in practice. Accordingly, it is desirable to study the architectural robustness of flow-based lossless compression models and address

such security concerns. While prior work (Pope, Balaji, and Feizi 2020) has shown that the flow model might become vulnerable under adversarial attack, there appears to be a restricted approach since their theoretical analysis is only based on the continuous flow models under simplified assumptions. By contrast, a deeper understanding of the architectural vulnerability of flow-based lossless compression models is still missing. Therefore, we raise the following questions: *Whether or not the inner architecture itself of a flow-based lossless compression model can expose more vulnerable to adversarial attacks? How can we design a robust lossless compression codec from an architectural robustness perspective?*

In this paper, we make the first attempt to identify the weakness of the multi-scale architecture adopted by many state-of-the-art flow-based lossless compression models, from an empirical and theoretical perspective. Specifically, We analyze the robustness of the multi-scale architecture via the Lipschitz property, which reveals the reason behind the fragile adversarial robustness. Based on the theoretical insight, we design a more powerful attack, i.e., auto-weighted projected gradient descent (AW-PGD) attack, to expose the more vulnerable endopathic controlled by the multi-Scale architecture. Although the multi-scale architecture is more vulnerable to adversarial attacks, we surprisingly find that the robustness of the rest of the model can be enhanced by such weakness. To achieve this we propose a novel lossless compression model named robust integer discrete flow (R-IDF). A method for constraining multiscale-architecture. Experiments show that R-IDF can significantly enhance the robustness of the model. For instance, the compression ratio is improved from 1.04 to 1.40 under PGD-10

Our main contributions can be summarized as follows:

- We present a more reasonable assumption for the flow model. Based on this, we prove an upper bound on the increase of negative log-likelihood under adversarial perturbation. Our theoretical results meets experimental expectations, and expose the architectural vulnerability of flow-based lossless compression models to the adversarial attack.
- Based on our theoretical analysis on the architectural robustness, we designed AW-PGD, which can effectively help the PGD attack to get out of the saddle point dilemma when generating adversarial samples. Our experiments show that AW-PGD is more effective and universal adversarial examples.
- We propose R-IDF, a regularization method for IDF, which achieves both reliable robustness and computational efficiency comparable to adversarial training. Compared with the clean model and the adversarial training model, its robustness is improved by 50% and 5%, respectively

Related Work

Flow-based lossless compression

According to Shannon’s source coding theory (MacKay et al. 2003), the limit of lossless compression is the entropy of the data distribution. Many efficient entropy coding

algorithms can approach or reach this lower bound (Huffman 1952; Witten, Neal, and Cleary 1987; Duda 2013), but only if we can explicitly evaluate the density functions. Deep models that can accomplish it can be divided into three categories. VAEs with Bits-Back technique (Townsend et al. 2019; Kingma, Abbeel, and Ho 2019) can be used for efficient lossless coding. However, VAEs model ELBO, which leads to a theoretical gap between the actual distribution. This prevents the compression rate from being improved further (Zhang et al. 2021b). Autoregressive models (Salimans et al. 2017; Chen et al. 2018), such as Pixel-CNN, maintain the best distribution estimation performance. However, the considerable time consumption caused by pixel-by-pixel inference makes the application unattainable. Some recent works implement local Autoregressive, which makes it achievable to accelerate inference for AR (Zhang et al. 2022; Zhang, Zhang, and McDonagh 2021). Continuous flows (Kingma and Dhariwal 2018; Dinh, Sohl-Dickstein, and Bengio 2016; Ho et al. 2019; Dinh, Krueger, and Bengio 2014; Chen et al. 2019) use a reversible network structure to model the bijection from the image space to the latent space, providing an precise estimation of the distribution and ensuring acceptable speed.

However, continuous flows cannot be directly used in compression tasks because of their numerical loss in quantization (Hoogeboom et al. 2019; Behrmann et al. 2021). Existing solutions for this can be divided into two categories. (Ho, Lohn, and Abbeel 2019; Zhang et al. 2021a) provides unique coding methods to efficiently encode the numerical loss caused by quantization. These methods can obtain slight quantization loss, but the specific continuous flow model they are based on (Ho et al. 2019) has inferior resistance to adversarial noise and is difficult to proceed with adversarial training. Another approach is to restrict the structure of the flow to ensure a strict bijection of the discrete data to the discrete base distribution (Hoogeboom et al. 2019; Berg et al. 2020; Zhang et al. 2021b). For example, IDF and IDF++ use the rounding operator, while IVPF uses volume-preserving flows. The disadvantage of this approach is that this constraint can confine the expressivity of the transformation.

Adversarial attack and defense

In the context of a classification task, adversarial examples are slight and malevolently designed perturbations that change a model prediction label. Existing adversarial attacks can be roughly separated into two types: white-box attacks (Carlini and Wagner 2017; Su, Vargas, and Sakurai 2019; Goodfellow, Shlens, and Szegedy 2014; Madry et al. 2017) and black-box attacks (Bhagoji et al. 2018; Dong et al. 2018, 2019). In the white-box scene, the parameters of the model can be obtained. While in the black-box setting, the adversary cannot fetch the model’s parameters. Here we mainly consider white-box attacks. Given a labeled data set $\mathcal{D} = \{(\mathbf{x}, y)\}_{i=1}^N$, adversarial example is aimed to change the prediction from DNN. (eg. $f(x) = y, f(x_{adv}) \neq y$), under the premise of guarantees $\|\mathbf{x}_{adv} - \mathbf{x}\|_{l_p} \leq \epsilon$. The commonly used white-box attack methods include the Fast Gradient Sign Method (FGSM) (Goodfellow, Shlens, and

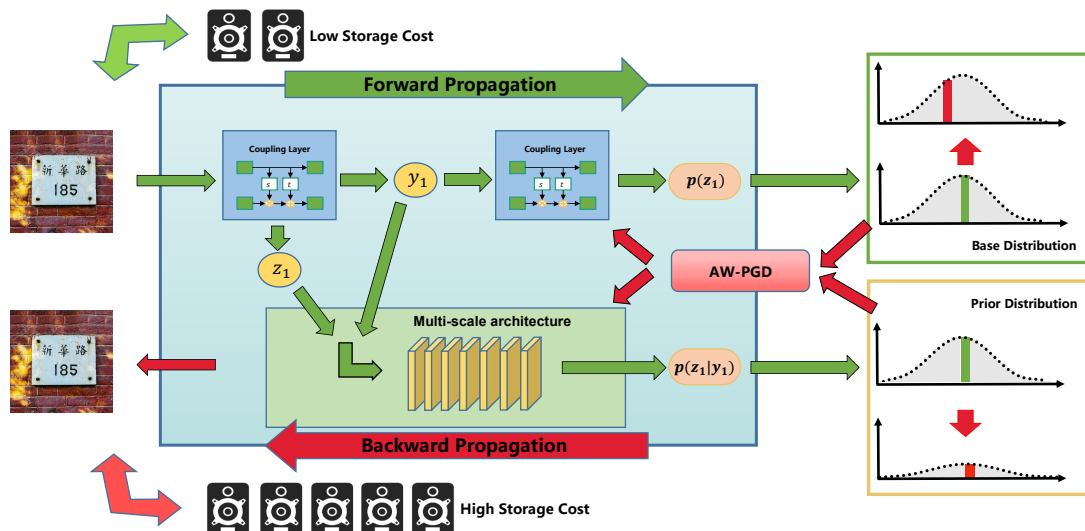


Figure 2: The full-scale pipeline of the proposed AW-PGD method against a flow-based model. Through Multiscale-architecture, the input image outputs multiple prior likelihoods and the likelihood of the base distribution. AW-PGD gives different weights to the gradients of varying likelihood loss to achieve the effect of concentrating on the attack of vulnerable modules. Note that the parameters of the base distribution are fixed, while the prior distribution parameters are predicted by CNN. As such, the adversarial attack works differently when attacking these two distributions.

Szegedy 2014),

$$\mathbf{x}_{adv} = \mathbf{x} + \alpha \cdot \text{sign}(\nabla_{\mathbf{x}} \ell(f(\mathbf{x}), y))$$

and projected gradient descent (PGD) (Madry et al. 2017),

$$\mathbf{x}_{adv}^{t+1} = \text{Proj}_{\epsilon}(\mathbf{x}_{adv}^t + \alpha \cdot \text{sign}(\nabla_{\mathbf{x}} \ell(f(\mathbf{x}_{adv}^t), y))) \quad (1)$$

PGD is equivalent to a multi-iteration version of FGSM and keeps the adversarial samples within the restricted domain utilizing a projection operator. The above attack methods have been verified to have sound effects on multiple data sets and different DNN networks.

There has been extensive research on improving the robustness of DNNs for defending against adversarial examples. One of the defense methods that can effectively withstand adversarial examples is adversarial training. The methodology of adversarial training can be seen as a min-max function optimization process:

$$\min_{\theta} \mathbb{E}_{(\mathbf{x}, y) \sim \mathcal{D}} \left[\max_{\delta \in \mathcal{S}} \ell(\theta, \mathbf{x} + \delta, y) \right]$$

The inner maximization is equivalent to the generation process of adversarial examples, and outer minimization tries to reduce the loss of the model on adversarial examples.

Nevertheless, little effort has been devoted to the robustness of generative models, especially flow-based models. (Nalisnick et al. 2018) indicates that flow may map OOD data to subdomains with high probability densities. (Behrmann et al. 2021; Cornish et al. 2020) found in the experiment that when the probability distribution of modeling is very complex, the flow will become pathological; that is, the hidden variable will leak mass outside of the support (Cornish et al. 2020). All of these imply the fragile robustness of flow from different perspectives. (Pope, Balaji,

and Feizi 2020) explores the robustness of the flow-based model for the first time and theoretically points out that both adversarial attacks and adversarial training are practical on flow. It is indicated from experiments that some widely-used flow-based models do not have satisfactory adversarial robustness. However, its theoretical analysis under strong assumptions limits it to finding more effective attack and defense methods.

Preliminaries

In this section, we begin with a brief introduction to the normalizing flow and its major components applied in lossless compression.

Flow-based Lossless Compression

Normalizing flow is generally designed as a learnable bijection $F: \mathcal{X} \rightarrow \mathcal{Z}$ from an unknown continuous distribution $p(\mathbf{x})$ to another tractable prior probability distribution $p(\mathbf{z})$, where $\mathbf{x} \in \mathcal{X}$ and $\mathbf{z} \in \mathcal{Z}$. To realize lossless compression with normalizing flows, the input data \mathbf{x} is transformed into the latent variable \mathbf{z} that is encoded with entropy coding by a prior probability distribution. Formally, the log likelihood of $p_{\mathcal{X}}(\mathbf{x})$ can be calculated by

$$\log p_{\mathcal{X}}(\mathbf{x}) = \log p_{\mathcal{Z}}(\mathbf{z}) + \log \left| \det \left(\frac{\partial \mathbf{z}}{\partial \mathbf{x}^T} \right) \right|$$

Coupling layer In order to model the bijective function $F(\cdot)$ efficiently, it can be decomposed into a combination of invertible coupling-layers, i.e., $F = f_L \circ f_{L-1} \circ \dots \circ f_1$. This requires that each layer in the flow-based model preserves the reversibility, and the determinant of the Jacobian

matrix of each f_l , $l = 1, 2, \dots, L$, is easy to calculate. For this purpose, there are two types of known coupling-layers applied to flow-based models:

- **Additive coupling layers:**

$$\begin{aligned} f(\mathbf{x})_{1:s} &= \mathbf{x}_{1:s} \\ f(\mathbf{x})_{s+1:C} &= \mathbf{x}_{s+1:C} + t(\mathbf{x}_{1:s}) \end{aligned} \quad (2)$$

- **Affine Coupling Layers:**

$$\begin{aligned} f(\mathbf{x})_{1:s} &= \mathbf{x}_{1:s} \\ f(\mathbf{x})_{s+1:C} &= \mathbf{x}_{s+1:C} \odot g(s(\mathbf{x}_{1:s})) + t(\mathbf{x}_{1:s}) \end{aligned} \quad (3)$$

Where $\mathbf{x} = [\mathbf{x}_{1:s}, \mathbf{x}_{s+1:C}]$, \odot denotes the hadamard product, and $s(\cdot)$ and $t(\cdot)$ are parameterized neural networks. g stands for scaling operation e.g., sigmoid or $\exp(\cdot)$.

Affine coupling layers is commonly considered to achieve better performance (Kingma and Dhariwal 2018) and is adopted by many advanced flow-based models.

Multi-Scale Architecture Note that a bijection demands that \mathbf{x} should have the same dimension as \mathbf{z} 's, this suggests that each f_l needs to remain the same. However, stacking more layers of f_l , $l = 1, 2, \dots, L$, leads to higher computational complexity by the curse of dimensionality. This fact conflicts with the original intention that deeper architecture can better approximate the image probability distribution in lossless compression. Multi-scale architecture provides a solution to this dilemma, which acts as the role of the skip-connection in ResNet. It allows the model to output \mathbf{z}_k with smaller subdimension directly via a factor-out layer after passing through some f_l , as shown in the figure. Specifically, multi-scale structure decomposes the hidden prior distribution \mathbf{z} into a product of multiple prior distributions $\{\mathbf{z}_i\}_{i=1}^k$, i.e.

$$\log p(\mathbf{z}) = \log p(\mathbf{z}_{k+1}) + \sum_{i=1}^k p(\mathbf{z}_i | \mathbf{z}_{t>i}) \quad (4)$$

$$= \log p(\mathbf{z}_{k+1}) + \sum_{i=1}^k p(\mathbf{z}_i | \mathbf{y}_i) \quad (5)$$

Where k stands for the number of *factor-out* layers. Many popular flow-based lossless models have been designed with this structure to obtain better convergence and reduced complexity. For simplicity, we call the module that maps \mathbf{x} to \mathbf{z}_{k+1} as *main-flow* in the sequel.

Entropy coding Given a n -dimensional discrete data \mathbf{x} , its probability density $p(\mathbf{x})$ is approximated by some probabilistic modelling technique. Entropy coding $EC(\cdot)$ is defined as an injective map that compress data losslessly to binary strings with minimum code length lower bounded by the entropy of $H(\mathbf{x})$ (MacKay et al. 2003). Furthermore, Kraft and McMillan (Kraft 1949; McMillan 1956) point out that we can obtain better lossless compression results by more effective density estimations, including the flow-based lossless compression methods considered in this paper.

Methodology

In this section, we provide some theoretical results to support the empirical results on the vulnerability of flow-based models. To understand the architectural robustness of the flow models, we first show that the *main-flow* module and *factor-out* module have different robustness by the well-known Lipschitz property. Then, we design a more robust integer discrete flow (R-IDF) based on the global Lipschitz property proved by Behrman et al (Behrman et al. 2021).

Robustness on the Multi-Scale Architecture

Next we introduce the well-known Lipschitz continuity for our subsequent analysis.

Definition 1 (Lipschitz Continuity).

A function $F(\cdot) : \mathbb{R}^n \rightarrow \mathbb{R}^n$ is called L -Lipschitz continuous if there exists a constant L such that for any $x_1, x_2 \in \mathbb{R}^n$, we have

$$\|F(x_1) - F(x_2)\| \leq L \|x_1 - x_2\| \quad (6)$$

where L is called the Lipschitz constant.

Noticed that *main-flow* and *factor-out* are two different modules of multi-scale architecture, we analyze their theoretical adversarial robustness, separately.

Robustness on the Factor-out Layer We define factor-out layer as: $f_s(\mathbf{y}, \mathbf{z}) = \log(p_{q_\phi}(\mathbf{z}))$, where q_ϕ stands for a prior distribution with parameters determined by $\mu_\phi(\mathbf{y})$, $\sigma_\phi(\mathbf{y})$. Here $\mu_\phi(\cdot)$ and $\sigma_\phi(\cdot)$ are two parameterized neural networks. In practice, q_ϕ is generally chosen as a Gaussian distribution or mixed logistic distribution. With the definition of a factor-out layer, we can obtain the following lemma, whose proof is provided in the appendix.

Lemma 1 Assume that the non-linear transformations $\mu_\phi(\cdot)$ and $\sigma_\phi(\cdot)$ are both L -Lipschitz. $\mathbf{y}, \mathbf{z} \in \mathcal{X} \subset \mathbb{R}^n$, $\|\mathbf{z}\|_\infty, \|\mu_\phi(\mathbf{y})\|_\infty$, and $\|\sigma_\phi(\mathbf{y})^{-1}\|_\infty$ are all bound by b . Let \mathbf{z} and \mathbf{z}^* be samples from $q_\phi(Z)$ and $q_\phi^*(Z^*)$, where $q_\phi(Z), q_\phi^*(Z^*)$ are normal distribution parameterized by $\{\mu_\phi(\mathbf{y}), \sigma_\phi^2(\mathbf{y})\}$ and $\{\mu_\phi(\mathbf{y}^*), \sigma_\phi^2(\mathbf{y}^*)\}$, respectively. If $\|\mathbf{y} - \mathbf{y}^*\|_2 \leq \delta$ and $\|\mathbf{z} - \mathbf{z}^*\|_2 \leq \delta$, then

$$|\log(p_{q_\phi}(\mathbf{z})) - \log(p_{q_\phi^*}(\mathbf{z}^*))| \leq L * \delta * \sqrt{n} * O(b^5) \quad (7)$$

Lemma3 implies that we must obey strict requirements to guarantee the robustness of the factor-out layer. For example, we not only require $\mu(\cdot), \phi(\cdot)$ to be L -Lipschitz but also control the norm of the outputs. Since the upper bound is determined by b^5 , the factor-out layer tends to exhibit insufficient robustness when the size of b is not regulated effectively, which reveals the fact that even if the robustness of the main-flow can be guaranteed, the factor-out layer is still vulnerable to adversarial attacks as shown in our subsequent experiments. Furthermore, Lemma 1 demonstrates that the lower bound on the robustness also depends on the dimension of \mathbf{z} . This suggests that the factor-out layer closer to the input, tends to be less robust and more vulnerable to adversarial attack, which is consistent with our experiment results.

Robustness on the Main-flow We define the main-flow as $f_m(\cdot) : \mathbf{x} \mapsto \mathbf{z}_{k+1}$. Under the assumption that the latent variable $\mathbf{z}_{k+1} \sim \mathcal{N}(0, I_n)$, we can derive a lower bound on the robustness of the main-flow in the appendix.

Lemma 2 Assume that $f_m(\cdot) : \mathbf{x} \mapsto \mathbf{z}$ is L -lipschitz, $\mathbf{x} \in \mathcal{X} \subset \mathbb{R}^n$, and $\mathbf{z} \sim \mathcal{N}(0, I_n)$. If $\|\mathbf{x}^* - \mathbf{x}\|_2 \leq \delta$, we have:

$$\log(p(\mathbf{z}^*)) - \log(p(\mathbf{z})) \geq -L\delta\|\mathbf{z}\|_2 - \frac{\delta^2}{2} \quad (8)$$

where $\mathbf{z} = f_m(\mathbf{x})$ and $\mathbf{z}^* = f_m(\mathbf{x}^*)$.

Note that when the flow can certify reversibility and the probability density of the hidden variable can be concentrated around the base distribution, we have $\|f_m(\mathbf{x})\|_2 = O(\|\mathbf{x}\|_2)$. In practice, the norm $\|\mathbf{x}\|_2$ is generally bound by 1, which provides the adversarial robustness guarantee by the Lipschitz property of f_m . Nevertheless, as shown in the following section, if we adopt the affine coupling layers to achieve more acceptable performance, the Lipschitz property of f_m become unattainable. Therefore, we need to consider the efficiency and robustness trade-off to design a more reasonable architecture of flow-based model.

	Affine	Additive	Multi-scale	BPD
Glow	✓	×	✓	3.39
Glow	×	✓	✓	3.42
Glow	×	✓	×	4.38 ↓
IDF-C	×	✓	✓	3.3
IDF-C	×	✓	×	4.31 ↓

Table 1: Evaluation for different modules in Glow and IDF-C (the continuous version of IDF)

Based on Lemma 1 and Lemma 2, we can prove the following theorem on the architectural weakness of the multi-scale architecture:

Theorem 1 Given a flow model defined as $F(\cdot)$, assume that $\mathbf{x} \in \mathcal{X} \subset \mathbb{R}^n$, $\|\mathbf{x}\|_2 \leq b \in \mathbb{R}^+$. If the main-flow $f_m(\cdot)$ is L_1 -Lipschitz, factor-out layers are all L_2 -Lipschitz and $\|\mathbf{x}_{pert} - \mathbf{x}_{clean}\|_2 \leq \delta$, then we have

$$\begin{aligned} & L(F(\mathbf{x}_{pert})) - L(F(\mathbf{x}_{clean})) \\ & \geq -\sum_i^k L_2\delta\sqrt{\dim_k} * O(b^5) - L_1\delta * O(b) - \frac{\delta^2}{2} \end{aligned} \quad (9)$$

where k stands for the number of factor-out layers, \dim_k is the input's dimension of k -th factor-out layer, $L(\cdot)$ denotes the negative log-likelihood.

Notice that we are focusing on mappings between discrete distributions, so we are not concerned about the Jacobian determinants' effect. This does not change our conclusions; see the appendix for further discussion.

Auto-Weighted PGD Attack (AW-PGD)

Based on the previous theoretical analysis, we choose Integer Discrete Flow (IDF) as our objective lossless compres-

sion model to design a new auto-weighted PGD attack (AW-PGD). More arguments on the remaining flow-based compression models can be found in the Appendix. Integer Discrete Flow (IDF) is a discrete flow model with multi-scale architecture. It consists of two factor-out modules that output the prior likelihood in stages. Notice that the PGD algorithm can be directly migrated to the flow-based model and obtain a pleasing attack effect. We first reformulate the prior likelihood output by the multiscale architecture as a multi-loss function:

$$\begin{aligned} LOSS_{IDF} &= -\sum_{i=1}^2 \log p(\mathbf{z}_i|\mathbf{y}_i) - \log p(\mathbf{z}_3) \\ &= loss_{fo1} + loss_{fo2} + loss_{mf}, \end{aligned} \quad (10)$$

where $loss_{fo1}$, $loss_{fo2}$, and $loss_{mf}$ denotes the loss outputted by the 1-st factor-out layer, 2-st factor-out layer, and main-flow, respectively. During the training stage, these three losses enjoy the same weight because they all contribute to the distribution estimation of the hidden variables, but the identical weight setting is not reasonable for the design of an adversarial attack.

In theory, Lemma 4 implies that the adversarial robustness of different modules that output $loss_{fo1}$, $loss_{fo2}$, and $loss_{mf}$ is entirely different, the lower bound of the factor-out Layer's robustness is influenced by the dimension size of the input variables. This motivates us to assign higher weight to modules with poorer robustness so that the direction of the adversarial attack is more biased towards this module. Therefore, we propose Auto Weight Projected Gradient Descent (AW-PGD), a method for weighting multi-loss in the process of iterative attack. In particular, we calculate the increment of separate loss in the i -th iteration of the PGD algorithm and assign particular weights based on this increment, then we obtain the overall loss as follows:

$$LOSS^i = w_{\Delta_{fo1}^i}^i loss_{fo1}^i + w_{\Delta_{fo2}^i}^i loss_{fo2}^i + w_{\Delta_{mf}^i}^i loss_{mf}^i,$$

where the increment is defined by

$$\Delta_j^i = \max(loss_j^i - loss_j^{i-1}, 0),$$

and the normalized weights is obtain by the softmax:

$$w_{\Delta_{fo1}^i}^i, w_{\Delta_{fo2}^i}^i, w_{\Delta_{mf}^i}^i = \text{Softmax}(\Delta_{fo1}^i, \Delta_{fo2}^i, \Delta_{mf}^i).$$

From another perspective, AW-PGD introduce the prior information of module robustness difference to adjust preferences during PGD attack. Note that the IDF ensures a bijective mapping from \mathbb{Z}^d to \mathbb{Z}^d . This denotes that an integer with 8 bits can represent the output component of any intermediate layer from 0 to 255. Therefore, when the AW-PGD algorithm is applied to IDF, we will specify an upper bound of 8 bits per dimension for each loss. Then we can set the loss to this upper bound when it exceeds. The full algorithmic process is provided in the **supplementary material**

Defense via Robust Integer Discrete Flow

To design a more robust integer discrete flow to defend the adversarial attack, we recall the Lipschitz property proved by Behrmann et al [(Behrmann et al. 2021), Theorem 2] that

the affine layers cannot guarantee global Lipschitz property, leading to poorer robustness compared with the additive layers. Therefore, we need to employ additive coupling layers to the main-flow structure, which guarantees global Lipschitz property and tighter Lipschitz bounds. Furthermore, we need to utilize multi-scale architecture to stack as many additive layers as possible to achieve comparable performance. To this end, the principle of our defense is an appropriate adjustment to make the multi-scale architecture robust via a regularization method, termed robust integer discrete flow (R-IDF).

Inspired by Lemma 1 that the local Lipschitz bound of multi-scale architecture is jointly controlled by $\|\mu_\phi(\mathbf{y})\|_\infty$, $\|\sigma_\phi(\mathbf{y})^{-1}\|_\infty$, and the Lipschitz property of the factor-out layer, we use the spectral norm regularization of the convolution kernel in the factor-out layer to ensure its Lipschitz property and make its output norms as small as possible. In practice, spectral norm regularization and weight decay are used to constrain the factor-out layer:

$$LOSS_R = LOSS_{IDF} + \rho_1 \|W_{fo}\|_2^2 + \rho_2 \sigma(W_{fo})^2, \quad (11)$$

where W_{fo} represents the parameter matrix of the fact-out layer, $\sigma(W)$ and $\|W_{fo}\|_2^2$ is the spectral norm, and ℓ_2 norm for W with coefficient (ρ_1, ρ_2) .

Since two factor-out layers in IDF have different robustness due to input dimension differences, we can obtain substantial robustness gains by applying the above constraint only to the first factor-out layer, and this constraint barely loses accuracy on clean samples. Furthermore, our regularization method can be combined with hybrid adversarial training. As shown in the subsequent experiments, the combination of R-IDF and the hybrid adversarial training can further improve the robustness of the model, making it equal to or even transcend the robustness of adversarial training without sacrificing the accuracy on clean samples.

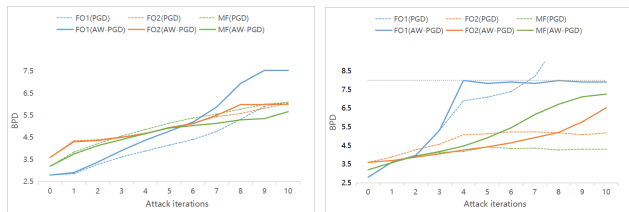
Experiment

Experiment setting

Datasets and Evaluation Metrics Following the settings in (Nalisnick et al. 2018; Pope, Balaji, and Feizi 2020), we verify the effectiveness of our methods over **CIFAR-10** (Krizhevsky, Hinton et al. 2009) and **SVHN** (Netzer et al. 2011) datasets. We adopt the standard metric in image explicitly probability modelling tasks and image compression tasks, Bits per dimension (BPD) and compression rate (CR), to evaluate the effectiveness of our method. BPD can be derived from NLL (negative log-likelihood). When the image has not undergone any compression operation, the BPD is 8. So the compression rate is 8/BPD. (We provide the implementation details in Sec.1 of the **Supplementary Material**).

Attack Evaluation

In this chapter, we verify the effectiveness of our attack against Integer Discrete Flow (IDF) and some most widely-adopted continuous flow models. Note that we also provide analysis for the transferability of the attack methods in Sec.2 of the **Supplementary Material**.



(a) perturbation $\epsilon = 1$

(b) perturbation $\epsilon = 2$

Figure 3: Evaluation results for AW-PGD.

Attack on IDF We first perform our proposed AW-PGD attack against IDF and compare it with the baseline method PGD. Note that due to the compression task, we set the bound in AW-PGD to 8. Fig. 3 shows that AW-PGD can concentrate the gradient on modules with inferior robustness even with small perturbation (i.e. $\epsilon = 1$). When the perturbation magnitude is higher (i.e. $\epsilon = 2$), the PGD algorithm will obsess over increasing $loss_{fo1}$ and ignore the gradients of other losses. Nevertheless, as mentioned before, the loss of more than 8-BPD does not result in an effective attack on the compression task. The specific attack effect is shown in Tab. 2, and we can see that AW-PGD has a significant improvement (38%) when $\epsilon = 1$, which demonstrates that our attack is extremely effective even over negligible perturbations. When the attack intensity becomes larger (i.e. $\epsilon \geq 2$), while the superiority of AW-PGD is partly masked by the fragile robustness of IDF, it still achieves the best results in all the experiments.

Attack Strength		CIFAR10	SVHN
$\epsilon=0$ (Clean sample)		2.41	3.79
$\epsilon=1$	AWPGD	1.24	1.36
	PGD	1.39	1.42
$\epsilon=2$	AWPGD	1.04	1.12
	PGD	1.05	1.17
$\epsilon=3$	AWPGD	1.02	1.10
	PGD	1.04	1.20

Table 2: Adversarial attack against IDF. *The evaluation metric is CR, where lower CR means worse result.*

Attack on continuous flow In this section, we will use PGD and AW-PGD for adversarial attacks on the continuous flow model. Note that Flow++ and Residual Flow do not utilise multi-scale architectures, so we did not implement AW-PGD for it. Firstly, it is shown in Table3 that none of these advanced flow models has acceptable adversarial robustness. Even if the PGD attack method is directly used, the output NLL will approach or even exceed 8 BPD at the attack strength $\epsilon \geq 2$. It indicates that those continuous flow models are challenging to design into robust compression algorithms. In contrast, R-IDF reveals significant robustness advantages under different attack strengths.

Additionally, Tab. 3 clearly shows that AW-PGD outperforms PGD on all models with multi-scale architecture.

CIFAR-10										
	Clean		Rand-Noise		PGD			AW-PGD		
	$\epsilon=0$	$\epsilon=1$	$\epsilon=2$	$\epsilon=3$	$\epsilon=1$	$\epsilon=2$	$\epsilon=3$	$\epsilon=1$	$\epsilon=2$	$\epsilon=3$
IDF-C	3.3	4.13	4.51	5.08	6.51	7.62	15.9	7.13	11.32	18.13
GLOW	3.39	4.21	4.63	5.11	6.6	14.12	25.31	7.62	17.54	28.27
RealNVP	3.53	4.35	4.59	4.87	6.82	7.47	8.14	6.91	7.64	8.16
Flow++	3.21	4.06	4.58	5.02	6.69	9.83	10.99	-	-	-
Residual flow	3.12	4.03	4.42	4.99	5.62	7.02	8.12	-	-	-
R-IDF	3.36	4.2	4.66	4.99	<u>4.91</u>	<u>5.71</u>	<u>5.92</u>	4.99	5.7	5.88

SVHN										
	Clean		Rand-Noise		PGD			AW-PGD		
	$\epsilon=0$	$\epsilon=1$	$\epsilon=2$	$\epsilon=3$	$\epsilon=1$	$\epsilon=2$	$\epsilon=3$	$\epsilon=1$	$\epsilon=2$	$\epsilon=3$
IDF-C	2.09	3.35	4.24	4.63	5.05	8.20	10.43	6.18	9.43	12.11
GLOW	2.12	3.25	4.10	4.59	6.23	25.46	60.71	8.91	27.19	71.23
RealNVP	2.30	3.15	3.85	4.38	5.12	6.82	7.89	5.57	7.26	8.25
R-IDF	2.17	3.3	4.01	4.57	<u>4.54</u>	<u>5.67</u>	<u>5.79</u>	4.54	5.65	5.80

Table 3: Evaluate PGD and AW-PGD attacks on continuous flow. The metric used here is BPD, with *higher values representing worse distribution estimation performance* of the model.

Without specifying the downstream task, the NLL outputted by the continuous flow is not limited as it is for the compressed task. It can be seen that AW-PGD can also show significant advantages when the attack intensity is high. Noticed that R-IDF strengthens the robustness of multi-scale architecture through regularization. Therefore, there is no significant difference between AW-PGD and PGD in attacking R-IDF task.

Defense Evaluation

We first implemented the two defense methods mentioned in (Pope, Balaji, and Feizi 2020), adversarial training and hybrid adversarial training, on IDF. We further evaluate the defense effect of our proposed R-IDF and R-IDF combined with hybrid adversarial training. The ablation study for R-IDF is provided in the Sec.2 of the **Supplementary Material**.

From Tab. 4, we can see that R-IDF has the highest compression ratio among all defense methods under clean samples and only decreases by about 1% compared to the clean model. It is worth noting that the training time of R-IDF (6.5min/epoch) is only 10 % compared with the adversarial training method (69min/epoch). However, its robustness is not significantly decreased compared with the adversarial training method. The R-IDF model combined with hybrid adversarial training can further improve the robustness, reaching or even exceeding the robustness of adversarial training. The compression rate on clean samples is improved by about 22% compared with adversarial training. Further, the adversarial training for Flow++ is 1100min/epoch, which is 170x and 16x that of R-IDF and Hybrid R-IDF, respectively. This shows that the effectiveness of adversarial training arises from unbearable training time cost.

Conclusion

We consider the architectural robustness of flow-based lossless compression models, focusing on the effect of the inner

CIFAR-10					
ϵ	CLEAN	Hybrid.	Adv	R-IDF	R-IDF [†]
0	2.41	2.27	1.85	2.38	2.27
1	1.35	1.67	1.70	1.63	1.78
2	1.04	1.57	1.60	1.40	1.63
3	1.03	1.55	1.57	1.35	1.57
4	1.01	1.51	1.51	1.34	1.52
5	1.00	1.39	1.44	1.32	1.44

SVHN					
ϵ	CLEAN	Adv.	Hybrid	R-IDF	R-IDF [†]
0	3.79	2.75	3.19	3.67	3.18
1	1.42	1.93	1.90	1.76	1.94
2	1.17	1.71	1.68	1.41	1.73
3	1.20	1.62	1.54	1.38	1.61
4	1.02	1.53	1.50	1.23	1.53
5	1.00	1.42	1.29	1.21	1.38

Table 4: Evaluation results for defense. The evaluation metric is CR, *where lower CR means worse result*. [†] stands for combination with hybrid adversarial training.

structures under adversarial attacks. Then we provide the theoretical analysis of the fragile robustness via the Lipschitz property. Inspired by the theoretical insights, we provide a new attack, AW-PGD, which often outperforms PGD. We also propose a new defense, R-IDF, a regularization method for multi-scale architecture, which is significantly more robust than other flow models while maintaining comparable model performance. On the experimental side, we verify that our proposed attack and defense methods are superior to the previous work. To the best of our knowledge, this is the first lossless compression method that takes the architectural robustness into account.

References

- Behrmann, J.; Vicol, P.; Wang, K.-C.; Grosse, R.; and Jacobsen, J.-H. 2021. Understanding and mitigating exploding inverses in invertible neural networks. In *AISTATS*, 1792–1800.
- Berg, R. v. d.; Gritsenko, A. A.; Dehghani, M.; Sønderby, C. K.; and Salimans, T. 2020. Idf++: Analyzing and improving integer discrete flows for lossless compression. *arXiv preprint arXiv:2006.12459*.
- Bhagoji, A. N.; He, W.; Li, B.; and Song, D. 2018. Practical black-box attacks on deep neural networks using efficient query mechanisms. In *ECCV*, 154–169.
- Carlini, N.; and Wagner, D. 2017. Towards evaluating the robustness of neural networks. In *2017 IEEE Symposium on Security and Privacy (SP)*, 39–57.
- Chen, R. T.; Behrmann, J.; Duvenaud, D. K.; and Jacobsen, J.-H. 2019. Residual flows for invertible generative modeling. *NIPS*, 32.
- Chen, X.; Mishra, N.; Rohaninejad, M.; and Abbeel, P. 2018. PixelSnail: An improved autoregressive generative model. In *International Conference on Machine Learning*, 864–872.
- Cornish, R.; Caterini, A.; Deligiannidis, G.; and Doucet, A. 2020. Relaxing bijectivity constraints with continuously indexed normalising flows. In *ICML*, 2133–2143.
- Dinh, L.; Krueger, D.; and Bengio, Y. 2014. Nice: Non-linear independent components estimation. *arXiv preprint arXiv:1410.8516*.
- Dinh, L.; Sohl-Dickstein, J.; and Bengio, S. 2016. Density estimation using real nvp. *arXiv preprint arXiv:1605.08803*.
- Dong, Y.; Liao, F.; Pang, T.; Su, H.; Zhu, J.; Hu, X.; and Li, J. 2018. Boosting adversarial attacks with momentum. In *CVPR*, 9185–9193.
- Dong, Y.; Pang, T.; Su, H.; and Zhu, J. 2019. Evading defenses to transferable adversarial examples by translation-invariant attacks. In *CVPR*, 4312–4321.
- Duda, J. 2013. Asymmetric numeral systems: entropy coding combining speed of Huffman coding with compression rate of arithmetic coding. *arXiv preprint arXiv:1311.2540*.
- Goodfellow, I. J.; Shlens, J.; and Szegedy, C. 2014. Explaining and harnessing adversarial examples. *arXiv preprint arXiv:1412.6572*.
- Ho, J.; Chen, X.; Srinivas, A.; Duan, Y.; and Abbeel, P. 2019. Flow++: Improving flow-based generative models with variational dequantization and architecture design. In *ICML*, 2722–2730.
- Ho, J.; Lohn, E.; and Abbeel, P. 2019. Compression with flows via local bits-back coding. *NIPS*, 32.
- Hoogeboom, E.; Peters, J.; Van Den Berg, R.; and Welling, M. 2019. Integer discrete flows and lossless compression. *NIPS*, 32.
- Huffman, D. A. 1952. A method for the construction of minimum-redundancy codes. *Proceedings of the IRE*, 40(9): 1098–1101.
- Kingma, D. P.; and Dhariwal, P. 2018. Glow: Generative flow with invertible 1x1 convolutions. *NIPS*, 31.
- Kingma, F.; Abbeel, P.; and Ho, J. 2019. Bit-swap: Recursive bits-back coding for lossless compression with hierarchical latent variables. In *ICML*, 3408–3417.
- Kraft, L. G. 1949. *A device for quantizing, grouping, and coding amplitude-modulated pulses*. Ph.D. thesis, Massachusetts Institute of Technology.
- Krizhevsky, A.; Hinton, G.; et al. 2009. Learning multiple layers of features from tiny images.
- MacKay, D. J., David JC; et al. 2003. *Information theory, inference and learning algorithms*. Cambridge university press.
- Madry, A.; Makelov, A.; Schmidt, L.; Tsipras, D.; and Vladu, A. 2017. Towards deep learning models resistant to adversarial attacks. *arXiv preprint arXiv:1706.06083*.
- McMillan, B. 1956. Two inequalities implied by unique decipherability. *IRE Transactions on Information Theory*, 2(4): 115–116.
- Nalisnick, E.; Matsukawa, A.; Teh, Y. W.; Gorur, D.; and Lakshminarayanan, B. 2018. Do deep generative models know what they don’t know? *arXiv preprint arXiv:1810.09136*.
- Netzer, Y.; Wang, T.; Coates, A.; Bissacco, A.; Wu, B.; and Ng, A. Y. 2011. Reading digits in natural images with unsupervised feature learning.
- Pope, P.; Balaji, Y.; and Feizi, S. 2020. Adversarial robustness of flow-based generative models. In *AISTATS*, 3795–3805.
- Salimans, T.; Karpathy, A.; Chen, X.; and Kingma, D. P. 2017. Pixelcnn++: Improving the pixelcnn with discretized logistic mixture likelihood and other modifications. *arXiv preprint arXiv:1701.05517*.
- Su, J.; Vargas, D. V.; and Sakurai, K. 2019. One pixel attack for fooling deep neural networks. *IEEE Transactions on Evolutionary Computation*, 23(5): 828–841.
- Townsend, J.; Bird, T.; Kunze, J.; and Barber, D. 2019. Hilloc: Lossless image compression with hierarchical latent variable models. *arXiv preprint arXiv:1912.09953*.
- Witten, I. H.; Neal, R. M.; and Cleary, J. G. 1987. Arithmetic coding for data compression. *Communications of the ACM*, 30(6): 520–540.
- Zhang, M.; Townsend, J.; Kang, N.; and Barber, D. 2022. Parallel Neural Local Lossless Compression. *arXiv preprint arXiv:2201.05213*.
- Zhang, M.; Zhang, A.; and McDonagh, S. 2021. On the out-of-distribution generalization of probabilistic image modelling. *NIPS*, 34: 3811–3823.
- Zhang, S.; Kang, N.; Ryder, T.; and Li, Z. 2021a. iflow: Numerically invertible flows for efficient lossless compression via a uniform coder. *NIPS*, 34: 5822–5833.
- Zhang, S.; Zhang, C.; Kang, N.; and Li, Z. 2021b. ivpf: Numerical invertible volume preserving flow for efficient lossless compression. In *CVPR*, 620–629.

Supplementary Material: Multi-Scale Architectures Matter: On the Adversarial Robustness of Flow-based Lossless Compression

Content Outline

This is the supplementary of "Multi-Scale Architectures Matter: On the Adversarial Robustness of Flow-based Lossless Compression". The content of this manuscript will be organized as following:

- **In Section 1** we provide details for experiment setting.
- **In Section 2** we provide the experimental evaluation of attack universality and ablation experiments of R-IDF.
- **In Section 3** we provide the full pseudocode of the AW-PGD algorithm.
- **In Section 4** we provide the details of the proofs of our main theoretical results on the robustness of flow models.
- **In Section 5** we provide more visualizations for the experiments in the main text.

Section 1: Experiment Detail

IDF, RealNVP were trained with default values given in their respective implementations. For **Glow** model evaluated on CIFAR10, we used the pretrained model. For **Glow** model evaluated on SVHN, we trained with default values given in the (Kingma and Dhariwal 2018). **Residual-flow** used pre-train model provided by (Chen et al. 2019). For **Flow++**, due to the limitation of GPU, we only use 4 batch-size while original setting is 64. Further, we implemented flow++ with only 400 training epochs. Although the model does not converge, according to (Ho et al. 2019), this already reflects the nature of the model.

We use ℓ_∞ as the bound in all attack and defense evaluations. For attack evaluation, we both use $iter = 10$ for PGD and AW-PGD. For defense evaluation, we select $(\rho_1, \rho_2) = (2, 0.5)$ as the regularization coefficient of R-IDF. Further, Adversarial training, Hybrid training, R-IDF(Hybrid), were all trained with $iter = 10$ and $\epsilon = 5$ attack iterations. According to (Pope, Balaji, and Feizi 2020), the mixing rate in Hybrid and R-IDF(Hybrid) are set to 0.5.

All the above experiments were training on two 2080Ti and all models are implemented in the PyTorch framework.

Section 2: More Experimental Results

Universality of adversarial samples Fig.4 shows the universality of adversarial samples generated by AW-PGD. We are doing the following experiments: 1) randomly pick one of the samples x from all test sets. 2) Generate adversarial noise x_Δ using that sample x . 3) Transfer the adversarial sample to other samples. 4) Calculate the perturbation of the image except x after being disturbed by x_Δ . 5) Repeat the above operation twenty times to calculate the average perturbation.

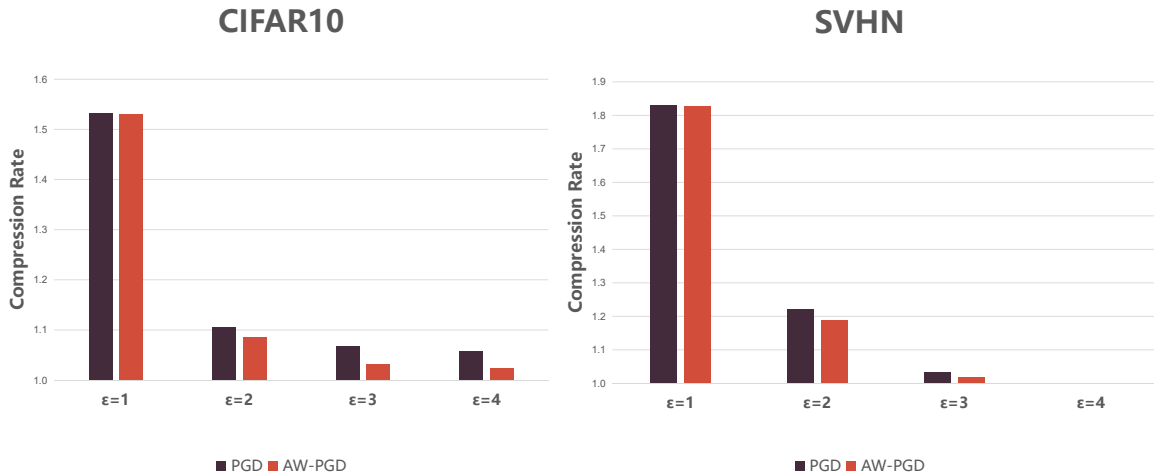


Figure 4: Visualization results for universality

As shown in the Table5, it is evident that the adversarial noise generated by AW-PGD lead to better universality. Although this phenomenon becomes less significant as the attack strength are too low, it still indicates that we can significantly reduce the compression effect of the model by transferring the weak adversarial noise generated on only part of the data to the rest of the data.

	CIFAR10		SVHN	
	PGD	AW-PGD	PGD	AW-PGD
$\epsilon=1$	1.5316	1.5296	1.8307	1.8265
$\epsilon=2$	1.1058	1.0852	1.2227	1.1871
$\epsilon=3$	1.0681	1.0322	1.0325	1.0192
$\epsilon=4$	1.0573	1.0234	1.0013	1.0005
$\epsilon=5$	1.0000	1.0000	1.0000	1.0000

Table 5: Evaluation results for universality. The evaluation metric is CR, where lower CR means worse result.

Ablation Study We ran the following ablations of our model: IDF vs R-IDF(weight decay only) vs R-IDF (spectral regularization only) vs R-IDF. The training parameters of all models are the same as above. As we can see in Figure5, the most significant effect is weight decay. Furthermore, the combination further improves robustness, indicating that the regularized constraints used in R-IDF are practical. It is also compatible with our theoretical analysis.

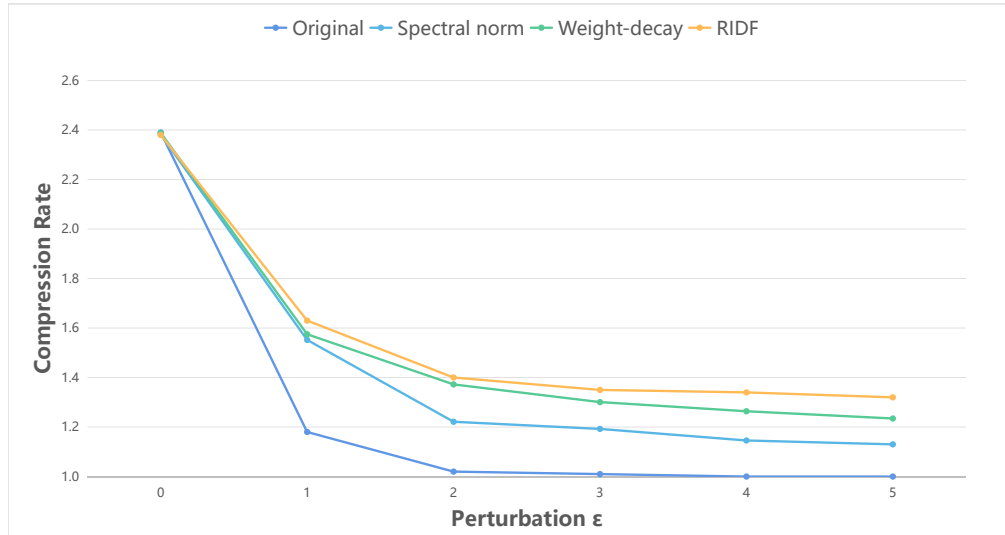


Figure 5: Ablation for R-IDF

Section 3: Algorithm Outline

We present the idea of the AW-PGD algorithm in the main text, and in this chapter, we will detail the workflow of the AW-PGD. AW-PGD introduce the prior information of module robustness difference by weighting multi-loss in the process of iterative attack.

Algorithm 1: Auto-Weighted Projected Gradient Descent

Input: The flow-base model $F(\cdot)$, the clean sample \mathbf{x} , attack strength ϵ , the number of iterations m , the steps size α , restriction of image compression $bound$

Output: adversarial sample $\mathbf{x}^* = \mathbf{x} + \delta_{\mathbf{x}}$

$loss_1^0, loss_2^0, loss_3^0 = F(\mathbf{x})$

while $i = 1, \dots, m$ **do**

$loss_1^i, loss_2^i, loss_3^i = F(\mathbf{x} + \delta_{\mathbf{x}}^i)$

if $loss_j > bound$ **then**

$loss_j = bound$

end if

$\Delta_j^i = \max(loss_j^i - loss_j^{i-1}, 0)$

$w_{\Delta_1}^i, w_{\Delta_2}^i, w_{\Delta_3}^i = \text{Softmax}(\Delta_1^i, \Delta_2^i, \Delta_3^i)$

$LOSS^i = \sum_{j=1}^3 w_{\Delta_j}^i loss_j^i$

$\delta_{\mathbf{x}}^i = \text{Proj}(\delta_{\mathbf{x}}^{i-1} + \alpha \cdot \text{sign}(\nabla_{\theta} LOSS^i))$

end while

Section 4: Proofs of Main Theoretical Results on the Robustness of Flow-based models

Lemma 3 : Assume the non-linear transformations $\mu_\phi(\cdot)$ and $\sigma_\phi(\cdot)$ are both L -Lipschitz. $\mathbf{x}, \mathbf{z} \in \mathcal{X}, \mathcal{X} \subset \mathbb{R}^n$. $\|\mathbf{z}\|_\infty \leq b_1$, $\|\mu_\phi(\mathbf{x})\|_\infty \leq b_2$, $\|\sigma_\phi(\mathbf{x})^{-1}\|_\infty \leq b_3$, $b_1, b_2, b_3 \in \mathbb{R}^+$, let $b = \max(b_1, b_2, b_3)$. Finally, let \mathbf{z} and \mathbf{z}^* be sampled from $q_\phi(Z)$ and $q_\phi^*(Z^*)$, where $q_\phi(Z)$, $q_\phi^*(Z^*)$ are normal distribution parameterized by $\{\mu_\phi(\mathbf{y}), \sigma_\phi^2(\mathbf{y})\}$ and $\{\mu_\phi(\mathbf{y}^*), \sigma_\phi^2(\mathbf{y}^*)\}$, respectively. If $\|\mathbf{y} - \mathbf{y}^*\|_2 \leq \delta$ and $\|\mathbf{z} - \mathbf{z}^*\|_2 \leq \delta$, $\delta \in \mathbb{R}^+$, then we have

$$|\log(p_{q_\phi}(\mathbf{z})) - \log(p_{q_\phi^*}(\mathbf{z}^*))| \leq L * \delta * \sqrt{n} * C(B) = L * \delta * \sqrt{n} * O(b^5)$$

where $C(B) = C_1(B) + C_2(B)$, $C_1(B) = (b_1 + b_2)^2 b_3^3 + (b_1 + b_2) b_3^2 + b_3$, and $C_2(B) = (b_1 + b_2) b_3$.

Proof 1 The original can be split into two parts by the absolute value inequality

$$|\log(p_{q_\phi}(\mathbf{z})) - \log(p_{q_\phi^*}(\mathbf{z}^*))| \leq |\log(p_{q_\phi}(\mathbf{z})) - \log(p_{q_\phi}(\mathbf{z}^*))| + |\log(p_{q_\phi}(\mathbf{z}^*)) - \log(p_{q_\phi^*}(\mathbf{z}^*))|$$

Firstly, we need to prove:

$$|\log(p_{q_\phi}(\mathbf{z}^*)) - \log(p_{q_\phi^*}(\mathbf{z}^*))| \leq l * \delta * \sqrt{n} * C_1(B)$$

Since q_ϕ and q_ϕ^* are both the normal distribution of the diagonal matrix with the covariance matrix, we have:

$$\begin{aligned} \left| \log(p_{q_\phi}(\mathbf{z}^*)) - \log(p_{q_\phi^*}(\mathbf{z}^*)) \right| &\leq \left| \sum_{i=1}^n \log \left(\frac{\sigma_\phi(\mathbf{x})_i}{\sigma_\phi(\mathbf{x}^*)_i} \right) \right| + \left| \sum_{i=1}^n \frac{(z_i^* - \mu_\phi(\mathbf{x})_i)^2}{2\sigma_\phi(\mathbf{x})_i^2} - \frac{(z_i^* - \mu_\phi(\mathbf{x}^*)_i)^2}{2\sigma_\phi(\mathbf{x}^*)_i^2} \right| \\ &\leq \left| \sum_{i=1}^n \log \left(\frac{\sigma_\phi(\mathbf{x})_i}{\sigma_\phi(\mathbf{x}^*)_i} \right) \right| + \left| \sum_{i=1}^n (z_i^* - \mu_\phi(\mathbf{x})_i)^2 \left(\frac{1}{2\sigma_\phi(\mathbf{x})_i^2} - \frac{1}{2\sigma_\phi(\mathbf{x}^*)_i^2} \right) \right| \\ &\quad + \left| \sum_{i=1}^n \frac{1}{2\sigma_\phi(\mathbf{x}^*)_i^2} ((z_i^* - \mu_\phi(\mathbf{x})_i)^2 - (z_i^* - \mu_\phi(\mathbf{x}^*)_i)^2) \right| \end{aligned}$$

For the first part, we have:

$$\begin{aligned} \left| \sum_{i=1}^n \log \left(\frac{\sigma_\phi(\mathbf{x})_i}{\sigma_\phi(\mathbf{x}^*)_i} \right) \right| &\leq \left| \sum_{i=1}^n (\sigma_\phi(\mathbf{x})_i - \sigma_\phi(\mathbf{x}^*)_i) \cdot \left(\frac{1}{\sigma_\phi(\mathbf{x})_i} \right)_{max} \right| \\ &\leq \sqrt{nb_3^2 \sum_{i=1}^n (\sigma_\phi(\mathbf{x})_i - \sigma_\phi(\mathbf{x}^*)_i)^2} \\ &\leq \sqrt{nb_3} \|\sigma_\phi(\mathbf{x}) - \sigma_\phi(\mathbf{x}^*)\|_2 = \sqrt{nl} \delta b_3 \end{aligned}$$

where the second inequality follows from the Cauchy inequality and Lagrange mean value theorem.

For the second part, we have:

$$\begin{aligned} \left| \sum_{i=1}^n (z_i^* - \mu_\phi(\mathbf{x})_i)^2 \left(\frac{1}{2\sigma_\phi(\mathbf{x})_i^2} - \frac{1}{2\sigma_\phi(\mathbf{x}^*)_i^2} \right) \right| &\leq \sum_{i=1}^n |(z_i^* - \mu_\phi(\mathbf{x})_i)^2| \left| \frac{1}{2\sigma_\phi(\mathbf{x})_i^2} - \frac{1}{2\sigma_\phi(\mathbf{x}^*)_i^2} \right| \\ &\leq \sqrt{nb_3^3 (b_1 + b_2)^2} \sqrt{\sum_{i=1}^n (\sigma_\phi(\mathbf{x})_i - \sigma_\phi(\mathbf{x}^*)_i)^2} \\ &\leq \sqrt{nb_3^3 (b_1 + b_2)^2} \|\sigma_\phi(\mathbf{x}) - \sigma_\phi(\mathbf{x}^*)\|_2 \\ &\leq \sqrt{nl} \delta b_3^3 (b_1 + b_2)^2 \end{aligned}$$

where the second inequality follows from the Cauchy inequality and Lagrange mean value theorem.

For the third part, we have:

$$\begin{aligned}
\left| \sum_{i=1}^n \frac{1}{2\sigma_\phi(\mathbf{x}^*)^2} ((z_i^* - \mu_\phi(\mathbf{x})_i)^2 - (z_i^* - \mu_\phi(\mathbf{x}^*)_i)^2) \right| &\leq \left| \frac{b_3^2}{2} \sum_{i=1}^n 2(\mu_\phi(\mathbf{x})_i - \mu_\phi(\mathbf{x}^*)_i) \cdot (z_i^* - \mu_\phi(\mathbf{x})_i)_{max} \right| \\
&\leq b_3^2 \sqrt{n(b_1 + b_2)^2 \sum_{i=1}^n (\mu_\phi(\mathbf{x})_i - \mu_\phi(\mathbf{x}^*)_i)^2} \\
&\leq \sqrt{n}(b_1 + b_2)b_3^2 \|\mu_\phi(\mathbf{x}) - \mu_\phi(\mathbf{x}^*)\|_2 \\
&\leq \sqrt{n}l\delta(b_1 + b_2)b_3^2
\end{aligned}$$

where the second inequality follows from the Cauchy inequality.

Hence, we obtain:

$$|\log(p_{q_\phi}(\mathbf{z}^*)) - \log(p_{q_\phi^*}(\mathbf{z}^*))| \leq \sqrt{n}l\delta b_3 + \sqrt{n}l\delta b_3^3(b_1 + b_2)^2 + \sqrt{n}l\delta(b_1 + b_2)b_3^2 = l * \delta * \sqrt{n} * C_1(B)$$

Secondly, we need to prove:

$$|\log(p_{q_\phi}(\mathbf{z})) - \log(p_{q_\phi}(\mathbf{z}^*))| \leq C_2(B)$$

According to the definition of Lipschitz continuous,

$$\|f(\mathbf{x}_1) - f(\mathbf{x}_2)\|_2 \leq K \|\mathbf{x}_1 - \mathbf{x}_2\|_2$$

is equivalent to

$$(\forall \mathbf{x} \in \mathcal{X}) \|\partial f / \partial \mathbf{x}\|_2 \leq K$$

Since

$$\begin{aligned}
(\forall \mathbf{x} \in \mathcal{X}) \|\partial \log(p_{q_\phi}(\mathbf{z})) / \partial \mathbf{z}\|_2 &= (\forall \mathbf{x} \in \mathcal{X}) \|\text{diag}(\sigma_\phi^2(\mathbf{x}))^{-1} (\mathbf{z} - \mu_\phi(\mathbf{x}))\|_2 \\
&\leq \sqrt{\sum_{i=1}^n b_3^2 (b_1 + b_2)^2} = \sqrt{n}(b_1 + b_2)b_3
\end{aligned}$$

As such

$$|\log(p_{q_\phi}(\mathbf{z})) - \log(p_{q_\phi}(\mathbf{z}^*))| \leq \sqrt{n}(b_1 + b_2)b_3 \|\mathbf{z} - \mathbf{z}^*\|_2 = l\delta\sqrt{n}(b_1 + b_2)b_3$$

Finally, we obtain:

$$\begin{aligned}
|\log(p_{q_\phi}(\mathbf{z})) - \log(p_{q_\phi^*}(\mathbf{z}^*))| &\leq |\log(p_{q_\phi}(\mathbf{z})) - \log(p_{q_\phi}(\mathbf{z}^*))| + |\log(p_{q_\phi}(\mathbf{z}^*)) - \log(p_{q_\phi^*}(\mathbf{z}^*))| \\
&= l\delta\sqrt{n}(C_1(B) + C_2(B)) = l\delta\sqrt{n}C(B)
\end{aligned}$$

Lemma 4 Assume that $f_m(\cdot) : \mathbf{x} \mapsto \mathbf{z}$ is L -lipschitz, $\mathbf{x} \in \mathcal{X} \subset \mathbb{R}^n$, and $\mathbf{z} \sim \mathcal{N}(0, I_n)$. If $\|\mathbf{x}^* - \mathbf{x}\|_2 \leq \delta$, we have:

$$\log(p(\mathbf{z}^*)) - \log(p(\mathbf{z})) \geq -L\delta\|\mathbf{z}\|_2 - \frac{\delta^2}{2}$$

where $\mathbf{z} = f_m(\mathbf{x})$ and $\mathbf{z}^* = f_m(\mathbf{x}^*)$.

Proof 2 Using Theorem 3.1 in (Pope, Balaji, and Feizi 2020), we obtain:

$$\begin{aligned} \log(p(\mathbf{z}^*)) - \log(p(\mathbf{z})) &= \log(p_{\mathcal{N}(0, I_n)}(f_m(\mathbf{x}^*))) - \log(p_{\mathcal{N}(0, I_n)}(f_m(\mathbf{x}))) \\ &\geq \frac{\|f_m(\mathbf{x}^*)\|_2^2}{2} - \frac{(\|f_m(\mathbf{x})\|_2^2)(1 + \frac{l\delta}{\|f_m(\mathbf{x})\|_2})^2}{2} \\ &= -(l\delta\|f_m(\mathbf{x}^*)\|_2 + \frac{\delta^2}{2}) = -L\delta\|\mathbf{z}\|_2 - \frac{\delta^2}{2} \end{aligned}$$

Since transformation f_m is L -Lipschitz, and $\|\mathbf{x}\|_2$ is bounded, so $f_m(\mathbf{x})$ is always bounded. Without loss of generality, $\|f_m(\mathbf{x})\|_2 \leq L * \|\mathbf{x} - \mathbf{0}\|_2 + \|f_m(\mathbf{0})\|_2 = O(b)$

Theorem 2 Given a flow model defined as $F(\cdot)$, assume that $\mathbf{x} \in \mathcal{X} \subset \mathbb{R}^n$, $\|\mathbf{x}\|_2 \leq b \in \mathbb{R}^+$. If the main-flow $f_m(\cdot)$ is L_1 -Lipschitz, factor-out layers are all L_2 -Lipschitz and $\|\mathbf{x}_{pert} - \mathbf{x}_{clean}\|_2 \leq \delta$, then we have

$$L(F(\mathbf{x}_{pert})) - L(F(\mathbf{x}_{clean})) \geq -\sum_i^k L_2\delta\sqrt{dim_k} * O(b^5) - L_1\delta * O(b) - \frac{\delta^2}{2}$$

where k stands for the number of factor-out layers, dim_k is the input's dimension of k -th factor-out layer, $L(\cdot)$ denotes the log-likelihood.

Proof 3 Since:

$$\begin{aligned} L(F(\mathbf{x}_{pert})) - L(F(\mathbf{x}_{clean})) &= \left(\sum_{i=1}^k (\log p(\mathbf{z}_i^{pert} | \mathbf{y}_i^{pert}) - \log p(\mathbf{z}_i^{clean} | \mathbf{y}_i^{clean})) \right) \\ &\quad + (\log p(\mathbf{z}_{k+1}^{pert}) - \log p(\mathbf{z}_{k+1}^{clean})) \\ &= \sum_{i=1}^k (Loss_{f_{foi}}(\mathbf{x}_{pert}) - Loss_{f_{foi}}(\mathbf{x}_{clean})) \\ &\quad + Loss_{mf}(\mathbf{x}_{pert}) - Loss_{mf}(\mathbf{x}_{clean}) \end{aligned}$$

Assume \mathbf{y}_t and \mathbf{z}_t is the input of t -th factor-out layer f_{foi} . Since the flow modules are Lipschitz continuous and $\|\mathbf{x}\|_2 \leq b$, $\|f_m(\mathbf{x})\|_2 \leq L * \|\mathbf{x} - \mathbf{0}\|_2 + \|f_m(\mathbf{0})\|_2 = O(b)$. As such, $\|\mathbf{y}_t\|_\infty \leq \|\mathbf{y}_t\|_2 \leq O(b)$ and $\|\mathbf{z}_t\|_\infty \leq \|\mathbf{z}_t\|_2 \leq O(b)$. Similarly, due to the Lipschitz continuous for f_{foi} , $\|\mu_\phi(\mathbf{x})\|_\infty, \|\sigma_\phi(\mathbf{x})^{-1}\|_\infty$ can be also bounded by $O(b)$.

For every $Loss_{f_{foi}}$ outputted by i -th factor-out layer f_{foi} , according to **Lemma3**, we obtain:

$$Loss_{f_{foi}}(\mathbf{x}_{pert}) - Loss_{f_{foi}}(\mathbf{x}_{clean}) = \log(p_{q_\phi^*}(\mathbf{z}_i^{pert}) - \log(p_{q_\phi}(\mathbf{z}_i^{clean})) \geq -L_2 * \delta * \sqrt{dim_i} * O(b^5)$$

Further, assume $f_{mf} : \mathbf{y}_k \mapsto \mathbf{z}_{k+1} \sim \mathcal{N}(0, I)$, similarly, \mathbf{z}_k can be bound by $O(b)$, using **Lemma4**:

$$Loss_{mf}(\mathbf{x}_{pert}) - Loss_{mf}(\mathbf{x}_{clean}) = \log p(\mathbf{z}_{k+1}^{pert}) - \log p(\mathbf{z}_{k+1}^{clean}) \geq -L_1 * \delta * O(b) - \frac{\delta^2}{2}$$

Hence:

$$L(F(\mathbf{x}_{pert})) - L(F(\mathbf{x}_{clean})) \geq -\sum_i^k L_2\delta\sqrt{dim_k} * O(b^5) - L_1\delta * O(b) - \frac{\delta^2}{2}$$

Note that in main-flow of continuous flows we also need to consider the effect of the Jacobian determinant. However, it is necessary to introduce bi-Lipschitz to ensure the local Lipschitz property of the Jacobian determinant.

Definition 2 (Lipschitz Continuity and bi-Lipschitz Continuity)

A function $F(\cdot) : \mathbb{R}^n \rightarrow \mathbb{R}^n$ is called L -Lipschitz continuous if there exists a constant L such that for any $x_1, x_2 \in \mathbb{R}^n$, we have

$$\|F(x_1) - F(x_2)\| \leq L \|x_1 - x_2\|$$

If an inverse $F^{-1} : \mathbb{R}^n \rightarrow \mathbb{R}^n$ and a constant $L^* = \text{Lip}(F^{-1})$ exists such that for all $y_1, y_2 \in \mathbb{R}^n$

$$\|F^{-1}(y_1) - F^{-1}(y_2)\| \leq L^* \|y_1 - y_2\|$$

holds, then F is called bi-Lipschitz continuous.

With the bi-Lipschitz Continuity, we obtain:

Lemma 5 Assume that $f_m(\cdot) : \mathbf{x} \mapsto \mathbf{z}$ is bi-Lipschitz with bound L and L^{-1} , $\mathbf{x} \in \mathcal{X} \subset \mathbb{R}^n$. If $\|\mathbf{x}^* - \mathbf{x}\|_2 \leq \delta$, we have:

$$\left| \log \left| \det \left(\frac{\partial \mathbf{z}^*}{\partial \mathbf{x}^{*\top}} \right) \right| - \log \left| \det \left(\frac{\partial \mathbf{z}}{\partial \mathbf{x}^\top} \right) \right| \right| \leq 2n \log(L)$$

Proof 4 To prove the Lipschitz bounds, we use the identity:

$$\text{Lip}(F) = \sup_{\mathbf{x} \in \mathbb{R}^n} \left\| \det \left(\frac{\partial \mathbf{z}}{\partial \mathbf{x}^\top} \right) \right\|_2$$

where $\|\cdot\|_2$ represents the spectral norm of the Jacobian matrix. Thus, we obtain that:

$$\begin{aligned} \left| \log \left| \det \left(\frac{\partial \mathbf{z}^*}{\partial \mathbf{x}^{*\top}} \right) \right| - \log \left| \det \left(\frac{\partial \mathbf{z}}{\partial \mathbf{x}^\top} \right) \right| \right| &\leq \left| \sum_i^n \log |\sigma_i(x)| + \sum_i^n \log |\sigma_i(x^*)| \right| \\ &\leq 2n \sup_{x \in \mathbb{R}^n} |\log \sigma_i(x)| = 2n \log(L) \end{aligned}$$

where $\sigma_i(x)$ denotes the i -th singular value of $\det \left(\frac{\partial \mathbf{z}}{\partial \mathbf{x}^\top} \right)$

Note that if F^{-1} cannot guarantee Lipschitz property, then the absolute value of the minimal eigenvalue of the determinant can be infinitely close to zero. This makes $|\log \sigma_i(x)|$ unbounded. By Theorem 2 in (Behrmann et al. 2021), the affine coupling layer does not guarantee the bi-Lipschitz property, but the additive layer does. This indicates that the robustness of affine layer is more fragile in continuous flow, which is consistent with the point we argue in the main text.

Section 5: Experimental Visualization

In this section, we visualize the attack evaluation of AW-PGD on IDF versus Glow. And we visualize our proposed defense methods: R-IDF and R-IDF (Hybrid).

Due to the limitation of the compression task, no significant gap with PGD is exhibited in Figure6, but this situation is mitigated on the Glow model attack, as shown in Figure7. Note that AW-PGD does not try to make a small number of samples large to improve the effectiveness of the attack but instead shifts the data distribution as a whole. Furthermore, from Figure 8, we can clearly see that our defense methods have significant robustness improvement. In particular, when the attack strength $\epsilon = 1$, R-IDF is not significantly inferior to the adversarial training based method.

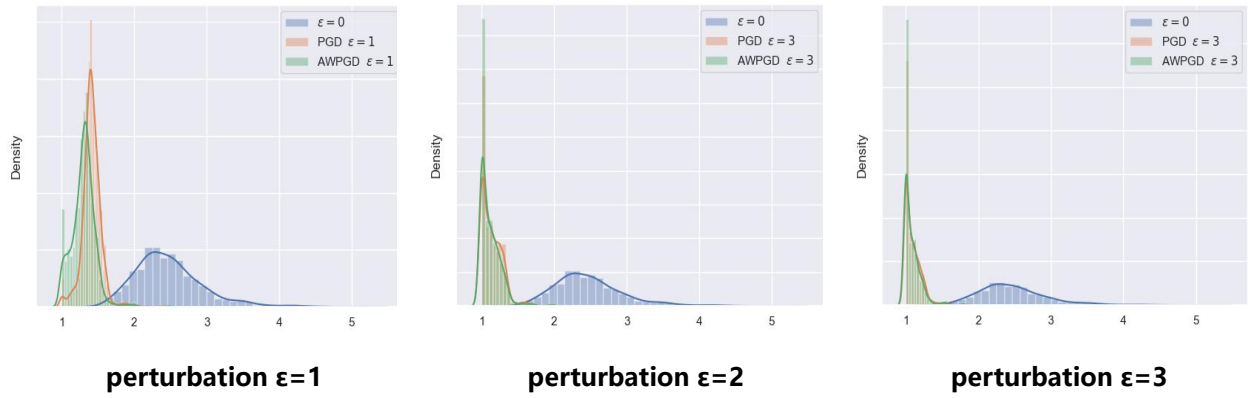


Figure 6: PGD & AW-PGD attack distributions for IDF. The x-label is CR, where lower CR means worse result.

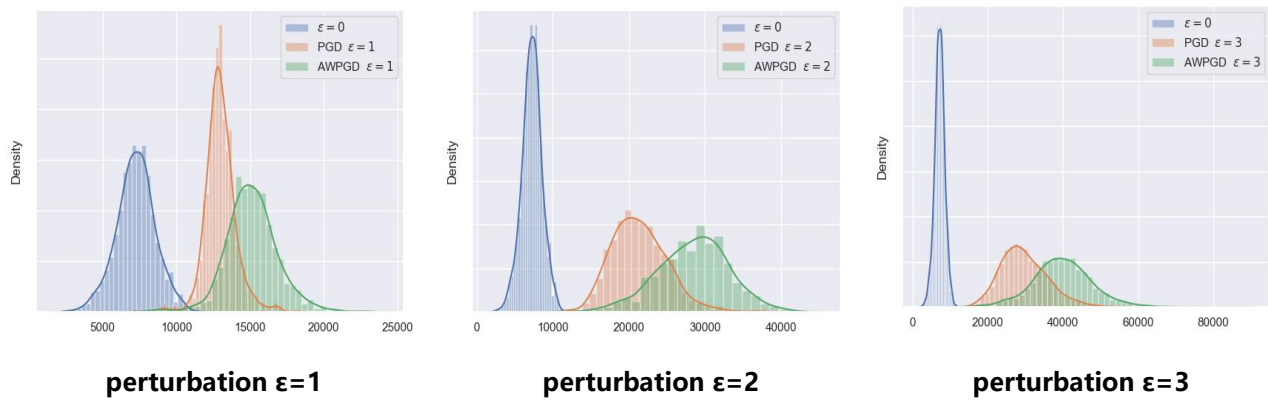


Figure 7: PGD & AW-PGD attack distributions for Glow. The x-label is NLL, where higher NLL means worse result.

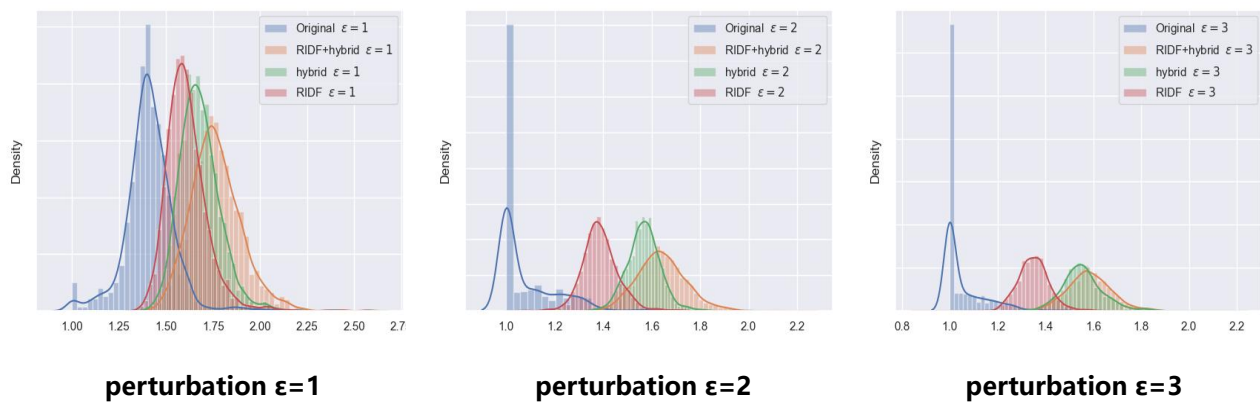


Figure 8: PGD attack distributions for IDF & R-IDF & R-IDF(hybrid). The x-label is CR, where lower CR means worse result.